Radiative Cooling Performance of a Converging Liquid Drop Radiator

Robert Siegel*
NASA Lewis Research Center, Cleveland, Ohio

The liquid drop radiator has been proposed in the literature as a possible lightweight device for dissipation of waste heat from power plants in space. The radiator consists of many directed streams of hot liquid drops that are cooled by passing through space and are then collected for reuse. To facilitate the collection of the cooled liquid, a converging geometry might be useful. As the streams converge toward the collector, the density and optical thickness of the droplet cloud are increased. The increase of optical thickness in the flow direction is shown to reduce the local emittance along the length of the radiator.

Nomenclature

a = absorption coefficient of absorbing-scattering region
c_p = specific heat of drop-filled region
$c_{p,d}$ = specific heat of drops
D = thickness of absorbing-scattering region
E_a, E_s = efficiency factors for absorption and scattering
E_1 = exponential integral function $\int_0^1 \mu^{-1} \exp(-x/\mu)\, d\mu$
I = source function in absorbing-scattering region, $\tilde{I} = \pi I/\sigma T_i^4$
N = number of drops per unit volume of layer
q_r = radiative heat flow per unit area and time
R_d = radius of spherical drop
R_o = outer radius parameter of region, $\sigma T_o^3(E_a + E_s)r_o/\rho_d c_{p,d} R_d \bar{u}$
r = radial coordinate opposite to flow direction
T = absolute temperature, $\tilde{T} = T/T_o$
T_m = integrated mean temperature across layer, $\tilde{T}_m = T_m/T_o$
T_o = value of T at $z = 0$
$\bar{u}$ = velocity of drops in layer
X = dimensionless coordinate x/D; X^* dummy variable of integration
x = coordinate across layer
Z = dimensionless coordinate $\sigma T_o^3(E_a + E_s)z/\rho_d c_{p,d} R_d \bar{u}$
z = coordinate in flow direction
ε = emittance of layer
ε_{fd} = emittance in fully developed region for cooling of a nonconverging layer
ε_{ut} = emittance for a uniform temperature distribution across layer thickness
Θ = total angular width of converging region
θ = angular coordinate of converging geometry
κ = optical coordinate $(a + \sigma_s)x$; κ^* dummy variable of integration
κ_D = local optical thickness along layer, $(a + \sigma_s)D$
ρ = density of drop-filled region
σ = Stefan-Boltzmann constant
σ_s = scattering coefficient of droplet layer
Ω = albedo for scattering, $\sigma_s/(a + \sigma_s)$

Subscripts

d = drop material
o = value at $z = 0$

Received Nov. 17, 1987; revision received Jan. 29, 1988.

*Research Scientist, Office of the Chief Scientist. Member AIAA.

Introduction

It is predicted that within the next 20 years there will be a considerable increase in demand for electrical power generating capability in space. The power requirements would be for space stations, military applications, orbiting communication systems, and commercial utilization of the space environment. For an orbiting power plant such as a solar dynamic or nuclear system, the waste heat from thermodynamic inefficiency must ultimately be dissipated by thermal radiation. This has led to current research for the development of lightweight radiators that can be more easily transported into space and then deployed. One system is the liquid drop radiator[1] in which many directed streams of hot liquid drops would be passed through space where they would lose part of their energy by direct exposure to the very cold space environment.

In the past several years, there have been a number of analytical and experimental investigations on the liquid drop radiator. A good summary of the current status is given in Ref. 2, which contains 49 references. In support of some work at our laboratory, the present author did some analyses of the radiative cooling behavior of drop-filled regions by using the methods of radiative transfer in absorbing and scattering regions.[3-4] The present work is a continuation of those analytical investigations and will examine the performance of a converging type of geometry, as illustrated in Fig. 1a. This configuration has certain advantages for the collection of the cooled drops by a rotating device that could function properly in a zero-gravity environment.

The analysis of radiative cooling of a semitransparent medium such as a cloud of drops, goes back at least 30 years and has been reviewed in the literature; a few of the significant references are Refs. 5–7. With scattering included, the equation of radiative transfer and the energy equation are solved simultaneously to yield the scattering source function and temperature distributions during the cooling process. For a converging geometry, the density of the medium and its optical thickness increase in the flow direction. If the region were locally at uniform temperature, the increase in optical thickness would tend to increase the local emittance toward a maximum value for each value of the scattering albedo. However, in the transient cooling situation, the outer portions of the region become cool relative to the inner portions, and this reduces the emissive ability based on the local mean temperature. This effect combines with the area reduction of the converging geometry to reduce the cooling ability relative to that for a nonconverging region.

Analysis

As shown in Fig. 1a, the droplet generator could be conveniently made in a modular form with a series of perforated

plates arranged in a circular fashion. The geometry can be analyzed in a cylindrical coordinate system as shown in Fig. 1b. All of the drops leave the generator with the same velocity $\bar{u}$, which remains unchanged as the droplet streams converge. The analysis neglects the effect of drop collisions. The thickness of the region D stays constant for the geometry chosen. The coordinate across the layer thickness is x, and in the flow direction it is z, which is opposite to the radial direction.

The conservation of mass in the radial direction for the differential control volume shown in Fig. 1b gives

$$\frac{\partial(\bar{u}\rho r)}{\partial r} = \bar{u}\frac{\partial(\rho r)}{\partial r} = 0 \tag{1}$$

since $\bar{u}$ remains constant along each droplet path. This shows that $\rho r = \text{constant} = \rho_o r_o$, the value at $z = 0$. Hence, the local density of the medium has an inverse relation to the radius

$$\rho(r) = \rho_o r_o / r \tag{2}$$

With regard to energy flow, the velocity $\bar{u}$ is assumed large enough so that temperature variations in the z direction are small compared with those in the x direction. The total width $r\Theta$ in the angular direction is assumed always large enough so that edge effects at $\theta = 0$ and Θ can be neglected. Then the energy equation balances the convective and radiative fluxes to give

$$-\bar{u}c_p\frac{\partial(\rho r T)}{\partial r} + r\frac{\partial q_r}{\partial x} = 0 \qquad T(x, r = r_o) = T_o \tag{3}$$

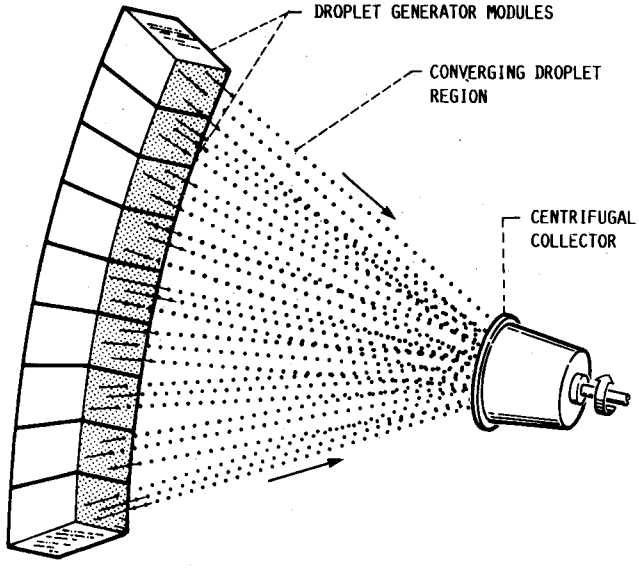

a) Configuration of converging radiator

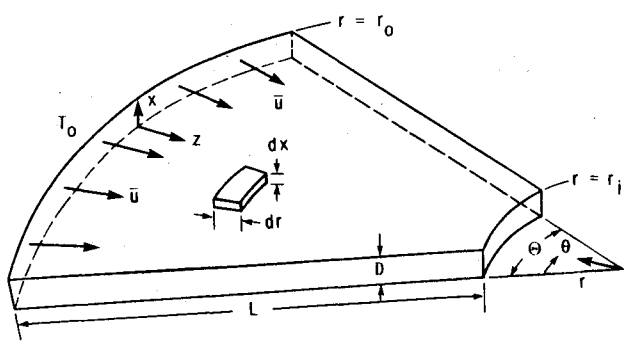

b) Model and coordinate system

Fig. 1 Geometry of converging liquid drop radiator.

Equation (2) shows that ρr is independent of radius, and so the energy equation simplifies to

$$\bar{u}c_p\rho(r)\frac{\partial T}{\partial r} = -\bar{u}c_p\rho_o r_o\frac{1}{r}\frac{\partial T}{\partial z} = \frac{\partial q_r}{\partial x} \tag{4}$$

An expression is now needed for the local radiative flux derivative in the x direction. In this geometry the temperature is decreasing in the z direction because of radiative cooling, the optical thickness is increasing in the z direction as the droplet number density increases, and the total width $r\Theta$ of the region is decreasing. The derivation of the local radiative flux derivative would be very complicated if all of these variations were included. However, in the space radiator, the thickness D is expected to be quite small compared with the radial or transverse $r\Theta$ dimensions. The rates of change of quantities in both the radial and θ directions are expected to be small compared with those in the x direction. Hence, the radiative surroundings at a location x,r are not expected to differ very much from those found locally in an infinite parallel plate geometry. It is thought that this assumption for the flux derivative will provide a reasonable approximation to the radiative cooling behavior without needing to perform a very complicated three-dimensional analysis. The local radiative flux derivative is then approximated by

$$-\frac{1}{a+\sigma_s}\frac{\partial q_r}{\partial x} = 2\pi\int_0^{\kappa_D} I(\kappa^*)E_1(|\kappa-\kappa^*|)\,d\kappa^* - 4\pi I(\kappa) \tag{5}$$

where a, σ_s, and κ_D are functions of r. Using the local plane layer approximation, the radiative source function I is related to the temperature by

$$I(\kappa,r) = (1-\Omega)\frac{\sigma T^4(\kappa,r)}{\pi} + \frac{\Omega}{2}\int_0^{\kappa_D} I(\kappa^*,r)E_1(|\kappa-\kappa^*|)\,d\kappa^* \tag{6}$$

By substituting the radiative flux, the energy equation can be written as

$$\bar{u}c_p\rho_o r_o\frac{1}{r}\frac{\partial T}{\partial z} = 4\pi(a+\sigma_s) \times\left[\frac{\kappa_D}{2}\int_0^1 I(X^*,Z)E_1(\kappa_D|X-X^*|)\,dX^* - I(X,Z)\right] \tag{7}$$

The extinction coefficient $a + \sigma_s$ depends on the local number density of the drops

$$a+\sigma_s = (E_a+E_s)\pi R_d^2 N(r) = (E_a+E_s)\pi R_d^2 N_o\frac{r_o}{r} \tag{8}$$

where the form at the right follows from the density relation in Eq. (2). In terms of droplet properties, the $\rho_o c_p$ is equal to

$$\rho_o c_p = \rho_d c_{p,d}(4/3)\,\pi R_d^3 N_o \tag{9}$$

Equations (8) and (9) are substituted into Eq. (7), and then Eqs. (6) and (7) are put into dimensionless form to yield

$$\frac{\partial\tilde{T}}{\partial Z} = 3\left\{\frac{\kappa_D(Z)}{2}\int_0^1 \tilde{I}(X^*,Z)E_1[\kappa_D(Z)|X-X^*|]\,dX^* - \tilde{I}(X,Z)\right\} \tag{10}$$

$$\tilde{I}(X,Z) = (1-\Omega)\tilde{T}^4(X,Z) + \kappa_D(Z)\frac{\Omega}{2} \times\int_0^1 \tilde{I}(X^*,Z)E_1[\kappa_D(Z)|X-X^*|]\,dX^* \tag{11}$$

If the integral is eliminated from Eqs. (10) and (11), Eq. (10) becomes

$$\frac{\partial \tilde{T}}{\partial Z} = 3\frac{1-\Omega}{\Omega}[\tilde{I}(X,Z) - \tilde{T}^4(X,Z)] \tag{12}$$

Since $\kappa_D = (a+\sigma_s)D$, the use of Eq. (8) shows that κ_D increases in the Z direction according to the relation

$$\kappa_D(Z) = \kappa_{D,o}\frac{r_o}{r} = \frac{\kappa_{D,o}}{1-(Z/R_o)} \tag{13}$$

When $\Omega > 0$, Eqs. (11) and (12) will be solved simultaneously for $\tilde{T}(X,Z)$ and $\tilde{I}(X,Z)$. When $\Omega = 0$, there is only absorption and emission by the drops (no scattering), and another form of the equations is used. For $\Omega = 0$, the relation $\tilde{I}(X,Z) = \tilde{T}^4(X,Z)$ is obtained from Eq. (11). This is substituted into the right side of Eq. (10) to yield for the condition of zero scattering (absorption and emission only)

$$\frac{\partial T}{\partial Z} = -3\left\{\tilde{T}^4(X,Z) - \frac{\kappa_D(Z)}{2} \times \int_0^1 \tilde{T}^4(X^*,Z)E_1[\kappa_D(Z)|X-X^*|]\,dX^*\right\} \tag{14}$$

As will be described, the energy relations are solved by numerical integration and $\tilde{T}(X,Z)$ is obtained. The quantity of principal interest is the mean temperature as a function of Z, as this shows how rapidly the droplet region is cooling. The energy carried by the flow at z, relative to the initial energy, is found by integrating the temperature distribution

$$\frac{\text{Energy at } z}{\text{Energy at } z=0} = \frac{\bar{u}\rho r\Theta c_p \int_0^D T(x,z)\,dx}{\bar{u}\rho_o r_o \Theta c_p T_o D}$$

By using Eq. (2), this simplifies to

$$\frac{\text{Energy at } Z}{\text{Energy at } Z=0} = \frac{1}{DT_o}\int_0^D T\,dx = \int_0^1 \tilde{T}(X,Z)\,dX = \tilde{T}_m(Z) \tag{15}$$

For comparison with these computed results, a simplified case will now be considered.

Simplified Case where $T(x,z)$ is Independent of x

In this instance it is assumed that the emittance can be approximated at each z location by the emittance for an absorbing and scattering plane layer at uniform temperature. This emittance, called ε_{ut}, is available in Ref. 3 for various values of κ_D and Ω. It is a function of z because of the variation of κ_D with z. An energy balance then gives

$$\bar{u}\rho c_p r\Theta D\frac{dT_m}{dz} = -2\varepsilon_{ut}(z)r\Theta\sigma T_m^4 \tag{16}$$

After using $\rho r = \rho_o r_o$, Eq. (16) is placed in dimensionless form to yield

$$\frac{4}{3}\kappa_{D,o}\frac{d\tilde{T}_m}{\tilde{T}_m^4} = -2\varepsilon_{ut}(Z)\left(1-\frac{Z}{R_o}\right)dZ \tag{17}$$

Integrating from $\tilde{T}_m = 1$ at $Z = 0$ to $\tilde{T}_m$ at Z yields

$$\tilde{T}_m = \left[1 + \frac{9}{2}\frac{1}{\kappa_{D,o}}\int_0^Z \varepsilon_{ut}(Z)\left(1-\frac{Z}{R_o}\right)dZ\right]^{-\frac{1}{3}} \tag{18}$$

The $\varepsilon_{ut}(Z)$ values correspond to the local optical thickness in the converging geometry Eq. (13). To evaluate Eq. (18) for a fixed value of the scattering albedo, the ε_{ut} at $\kappa_D(Z)$ was interpolated from Table 1 in Ref. 3 by use of a spline fit computer subroutine. For comparison, results for a nonconverging region with a uniform temperature distribution across its thickness can be found by letting $R_o \gg Z$ in Eq. (18) to obtain

$$\tilde{T}_m = \left(1 + \frac{9}{2}\varepsilon_{ut}\frac{Z}{\kappa_{D,o}}\right)^{-\frac{1}{3}} \tag{19}$$

In this instance ε_{ut} remains fixed at the value corresponding to $\kappa_{D,o}$ and Ω.

Numerical Solution

When scattering is included ($\Omega > 0$), Eqs. (11) and (12) are solved simultaneously for $\tilde{I}(X,Z)$ and $\tilde{T}(X,Z)$. The layer thickness from $X = 0$ to 1 was divided into evenly spaced increments. Usually, 40 ΔX intervals were used. Some of the results were checked by using 60, 80, and 100 intervals. Starting with the specified initial condition $\tilde{T}(X,0) = 1$, Eq. (11) was solved by iteration. To begin the iteration, the $\tilde{I}(X,0)$ was set equal to unity, and this was substituted into the integral on the right side to yield a new $\tilde{I}(X,0)$ value for each X. The difference between this $\tilde{I}$ and the trial $\tilde{I}$ was multiplied by an acceleration factor of 1.4, and the result added to the trial $\tilde{I}$ to obtain the new $\tilde{I}$ used for the next iteration. The acceleration factor of 1.4 was found by trial to give the most rapid convergence rate. The iteration was continued until the maximum relative change in $\tilde{I}$ at any X was less than 0.5×10^{-4}. Some of the calculations were checked by using one-tenth of this value. The $\tilde{I}$ and $\tilde{T}$ were then substituted into the right-hand side of Eq. (12), and the $\partial\tilde{T}/\partial Z$ at each X was used to extrapolate $\tilde{T}(X,Z)$ forward to the next Z location. A small ΔZ value in the range of 0.01 was used to start the calculations from $Z = 0$. As Z increased, the cooling rate decreased, and the size of ΔZ was gradually increased during the solution whenever ΔT_m decreased below a specified small value such as 0.005. The results were checked for typical cases by using smaller ΔZ and ΔX increments. When $\Omega = 0$, Eq. (14) was solved in a similar manner, except that an iteration loop was not required at each Z. The solution was carried forward until Z reached $0.9R_o$ or until $\tilde{T}_m$ decreased to 0.65.

To carry out the numerical solution, an accurate integration subroutine was required, and it must account for the singularity where $E_1(0) = \infty$. As described in Refs. 3 and 4, a Gaussian numerical integration routine was used, and the relations were integrated analytically in a very small X increment adjacent to the singularity. For a given $\kappa_{D,o}$, R_o, and Ω, the solution for $\tilde{T}(X,Z)$ and $\tilde{I}(X,Z)$ required 5 min or less on an IBM 370 computer when 40 ΔX intervals were used.

Results and Discussion

The result of principal interest is how rapidly the converging droplet layer cools as a function of distance from the droplet generator. The governing parameters are the initial optical thickness of the layer $\kappa_{D,o}$, the dimensionless maximum radial dimension R_o, and the scattering albedo Ω. To show the effect of these independent parameters, some groups of cooling curves will be given; then some simplified solutions will be used to help interpret the results. This will also show the conditions where the approximate solutions can be utilized to yield accurate results in a simple way. After discussing the cooling curves, the local emittance of the layer will be examined and compared with some special cases. This will reveal some of the basic physics for the radiative cooling of a region in which the optical

thickness is changing as the cooling proceeds.

Figure 2 gives the dimensionless mean temperature T_m/T_o as a function of Z for various values of R_o. This temperature ratio is equal to the fraction of the energy remaining in the layer at Z. Each part of the figure is for a different initial optical thickness $\kappa_{D,o}$.

Figure 2a is for a rather small initial optical thickness $\kappa_{D,o} = 1$; it shows the cooling behavior for three R_o values and for the limit $R_o \to \infty$, which is for a geometry that is not converging. The curves are extended to $Z = 0.8R_o$ (except, of course, for $R_o \to \infty$). The maximum cooling at each Z is for the nonconverging case, and the cooling rate progressively decreases as R_o is decreased. For purposes of discussion, think of $\bar{u}$ and the droplet generator width $r_o\Theta$ as being fixed in size. Then, decreasing R_o corresponds to the geometry being increasingly convergent, as illustrated on the figure. The decrease in cooling rate with decreasing R_o results from having less outer surface area for the converging layer, and also follows from the thickening of the layer optically as it converges. The inset in Fig. 2a is not as useful to visualize the behavior when the radiator geometry remains fixed, whereas the parameter R_o changes as a result of changing the droplet velocity. As $\bar{u}$ increases, corresponding to a decrease in R_o, there is less droplet transit time available for cooling, and hence there is a smaller decrease in T_m/T_o over the length of the radiator, as shown by the curves. As will be discussed later, the increase of κ_D with Z leads to a decreased local emittance rather than to an increase, as would be expected for a layer having a locally uniform temperature distribution across the thickness D. The solid and dashed lines on the figure show the effect of the scattering albedo. For $\Omega = 0$ there is only absorption and emission. When scattering is present, $\Omega = 0.6$, the amount of cooling is significantly decreased. This is expected from the decreased particle emission associated with drops that are more highly reflecting.

Figure 2b gives similar results for the initial optical thickness increased to $\kappa_{D,o} = 2$. Since $\kappa_{D,o}$ contains the number density and thickness N_oD, the layer in Fig. 2b contains twice the mass and initial internal energy as that in Fig. 2a; hence, the Z values to reach the same fractional energy loss are expected to be about twice as large. For the thicker layer, the scattering has a diminished influence, and the solid and dashed curves are somewhat closer together than in Fig. 2a.

The previous trends are continued on Fig. 2c where the initial optical thickness is doubled again to $\kappa_{D,o} = 4$. The effect of scattering has now significantly diminished. For Z values twice those in Fig. 2b, the $T_m(Z)/T_o$ values are not as small as those for $\kappa_{D,o} = 2$, and so the cooling process is not as efficient as for $\kappa_{D,o} = 2$.

Figure 2 provides results for only two values of the scattering albedo. To further examine the effect of scattering, results are given in Fig. 3 for several values of Ω for each of two values of $\kappa_{D,o}$ and R_o. For comparison, results (the dashed curves) are included for a nonconverging geometry ($R_o \to \infty$). As Ω increases above 0.6, there is a substantial decrease in cooling, since the droplets become poorly emitting and more highly reflective. As previously shown, the influence of scattering diminishes as $\kappa_{D,o}$ increases. A study of the results indicates that a $\kappa_{D,o}$ of about 2–3 is probably desirable if the droplet albedo is in the approximate range 0–0.3. For higher albedos, the temperature distribution becomes more uniform, and a larger $\kappa_{D,o}$ can be used, such as 4. The behavior is related to the locations of the maximum values that will be noted on Fig. 5b.

The purpose of Fig. 4 is to compare the solution with results obtained by using the simplified solution in Eq. (18). From the geometry, the local optical thickness as a function of Z is obtained from Eq. (13). Then from the results in Ref. 3 (as will be shown in Fig. 5a), the ε_{ut} for each local κ_D, and for the particular Ω value, is obtained for the converging radiating layer assumed to have a uniform temperature distribution across its thickness. These ε_{ut} values are used in Eq. (18) to obtain the T_m/T_o variation with Z. These approximate results are the dashed curves in Fig. 4. The results in Fig. 4a for $\kappa_{D,o} = 2$

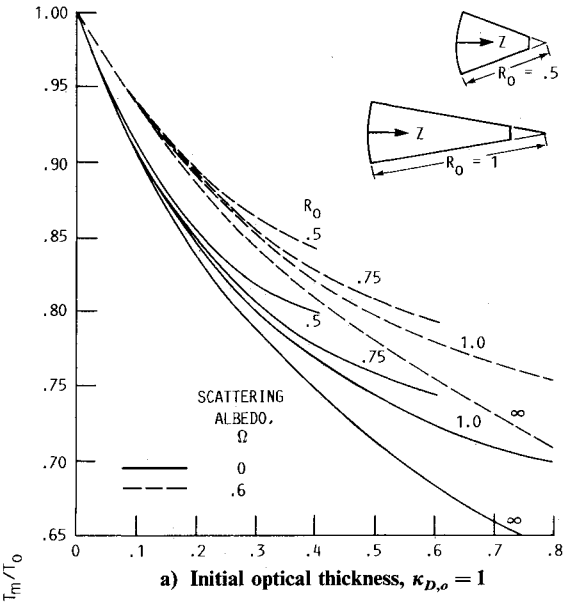

a) Initial optical thickness, $\kappa_{D,o} = 1$

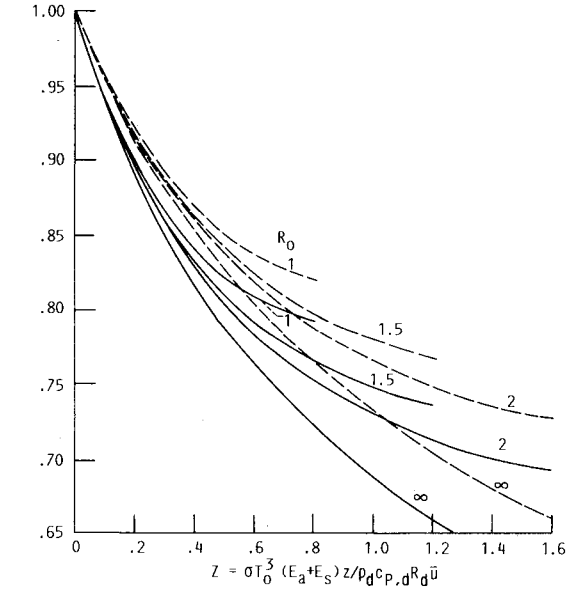

b) Initial optical thickness, $\kappa_{D,o} = 2$

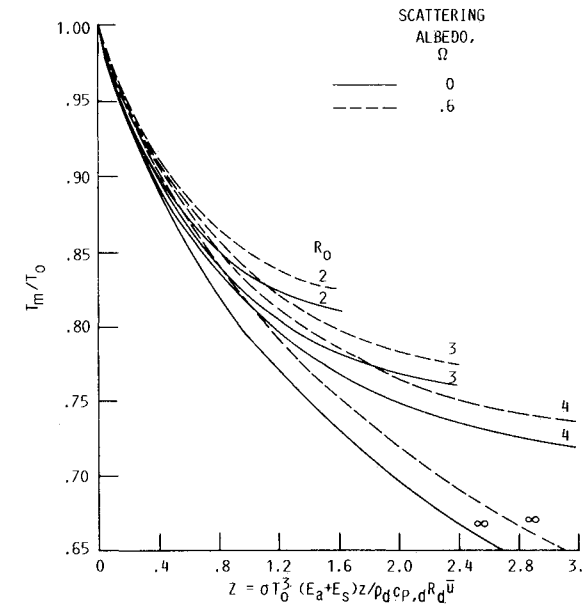

c) Initial optical thickness, $\kappa_{D,o} = 4$

Fig. 2 Cooling curves for a converging droplet layer.

show that very good agreement is obtained. Better than 2% agreement is obtained when $\Omega = 0$, whereas for $\Omega = 0.6$ the approximate results are essentially the same as the solution numerically computed from the basic energy equations. A higher value of Ω tends to make the temperature distribution more uniform across the layer thickness because of equalizing the distribution of energy by means of multiple reflections. Hence, closer agreement is obtained with the simplified solution that uses a uniform temperature distribution. The agreement is also closer as $\kappa_{D,o}$ is decreased below 2, since the temperature distribution becomes more uniform with decreasing optical thickness.

When $\kappa_{D,o}$ is increased to 4, Fig. 4b, there is a more significant deviation of the approximate solution from the numerically computed results where the temperature is a function of both X and Z. The approximate solution yields a more rapid cooling. The cooling behavior will now be interpreted in more detail by examining the variation of the layer emittance during the cooling process.

Before examining the emittance values from the numerical solution, the sets of ε values from Refs. 3 and 4 will be briefly reviewed. Figure 5a shows the ε_{ut} as a function of κ_D; these values are for a plane layer with a uniform temperature distribution. For each value of Ω, the ε increases as the optical thickness is increased. In contrast, Fig. 5b shows the ε_{fd} values that are reached during the transient radiative cooling of a plane layer that is initially at uniform temperature, and is then placed in very low temperature surroundings. These values are obtained after about 30% of the energy is lost. At that point it was found that the solution reaches a "fully developed" similarity condition and the emittance becomes constant at a ε_{fd} value for each Ω and κ_D. The behavior of ε_{fd} for a fixed Ω is that it reaches a maximum value as κ_D is increased and then decreases for larger κ_D. The decrease of ε_{fd} is the result of the

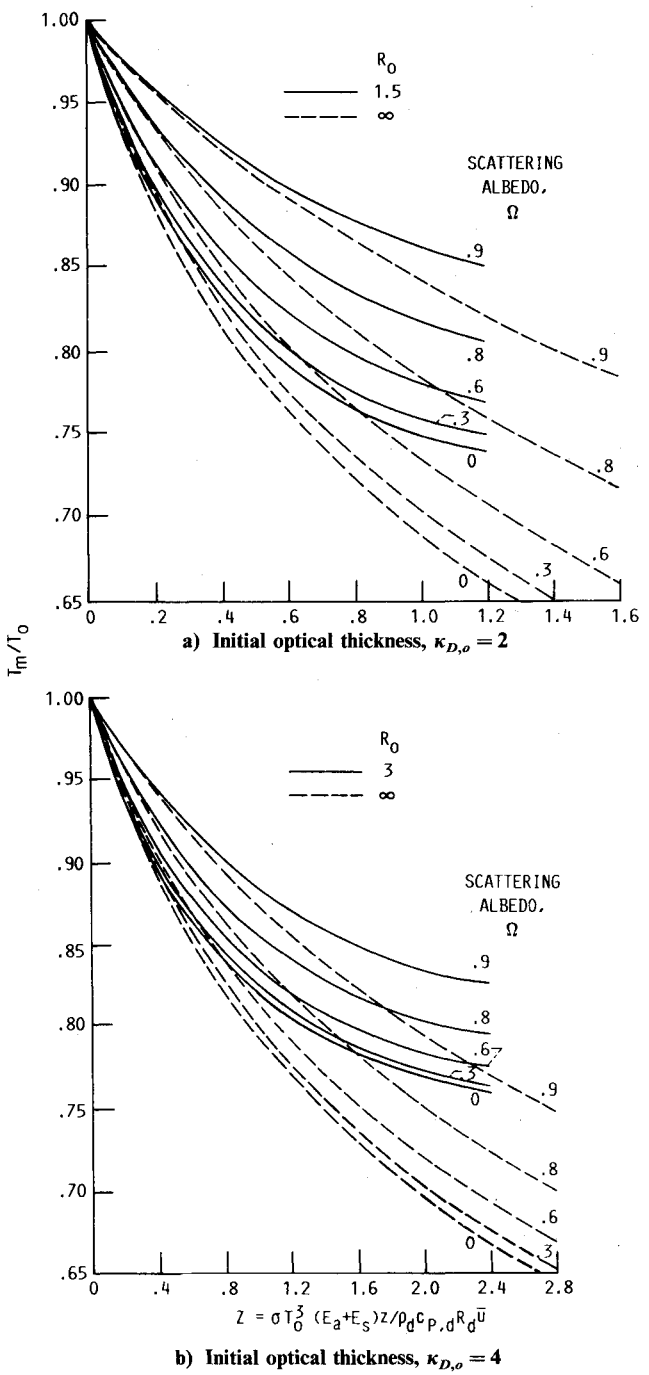

Fig. 3 Effect of scattering on cooling curves for converging droplet layer.

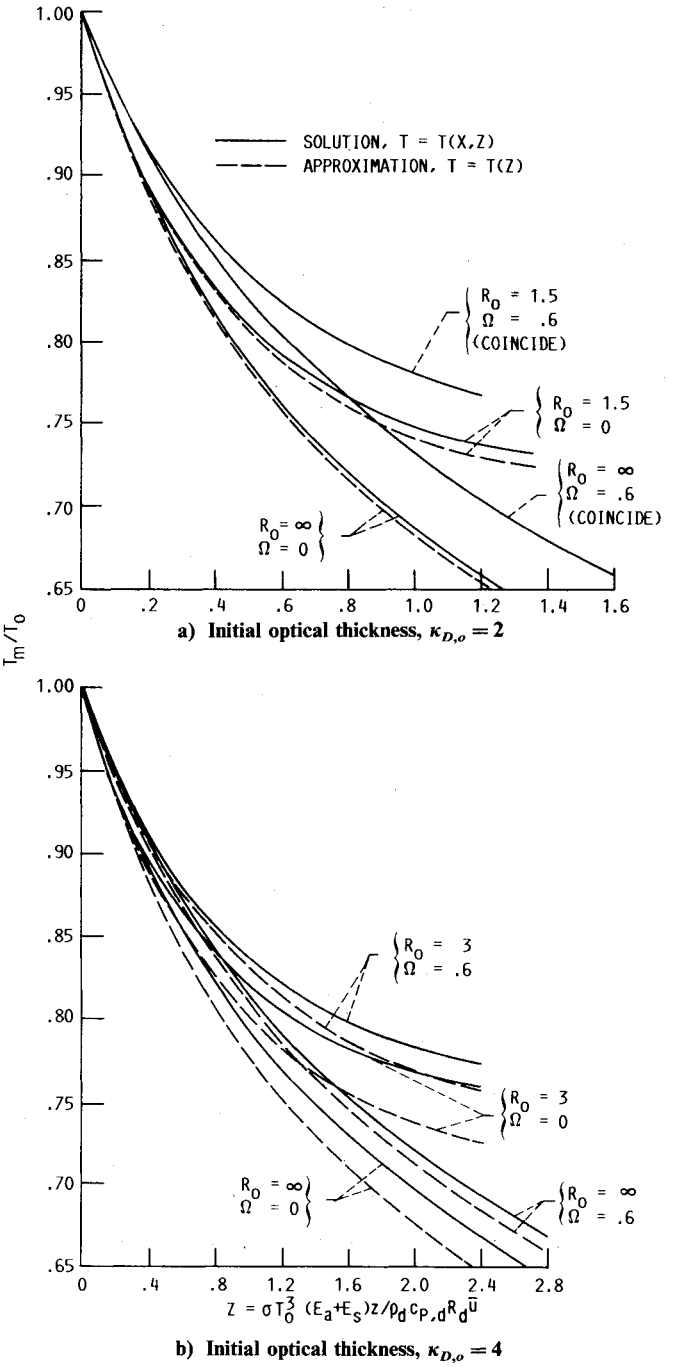

Fig. 4 Comparisons with simplified case of locally uniform temperature distribution.

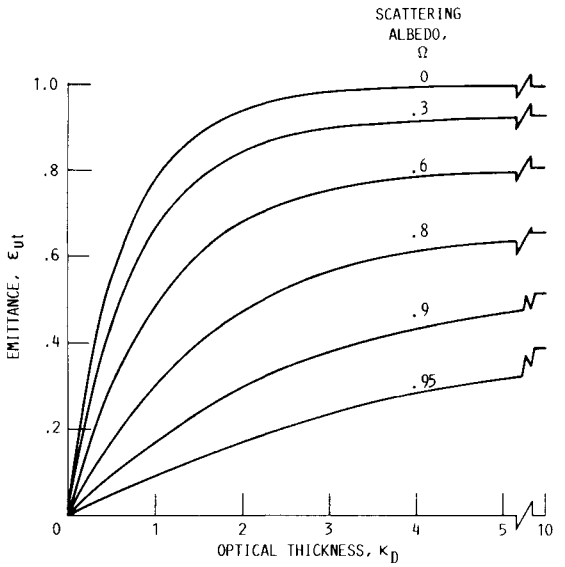

a) Emittance for uniform temperature layer

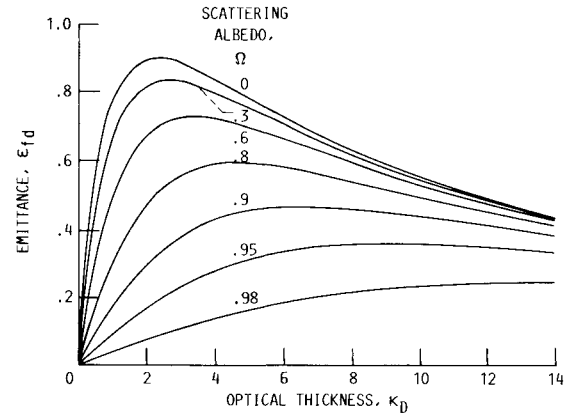

b) Emittance in fully developed region

Fig. 5 Emittance of absorbing-scattering plane layer.

nonuniformity of the temperature distribution that develops during cooling, and the subsequent relatively poor radiation from the outer region of the layer that has become cool.

Figure 6 shows local emittance values for the converging geometry. This emittance is the local heat flux leaving one side of the layer, divided by σT_m^4, where T_m is the local mean temperature. The three parts of Fig. 6 are for different values of the parameters. Consider Fig. 6c as an example, with $\kappa_{D,o} = 4$ and $\Omega = 0.6$. From the numerical solution of the energy equations, the emittance variation with Z is found as the solid line that decreases substantially with Z. At the top of the figure is shown the variation of κ_D, which increases with Z as given by Eq. (13). The uppermost dashed curve is ε_{ut}, obtained from Fig. 5a for a uniform temperature distribution at each Z. The ε_{ut} increases with Z because of the increase in the local κ_D. The next lower dashed curve on Fig. 6c is the solution for a nonconverging geometry as obtained by letting $R_o \to \infty$ in the present numerical analysis. Since the layer originates at uniform temperature, the initial ε is the same as that on Fig. 5a. Then as Z increases, the ε decreases toward the value for fully developed conditions given on Fig. 5b. The lowest dashed curve on Fig. 6c is obtained by using Fig. 5b locally along the channel; the ε_{fd} values correspond to the local κ_D values at the top of Fig. 6c. This lowest dashed curve is thus based on the condition that the temperature profile could achieve, for each Z, the similarity

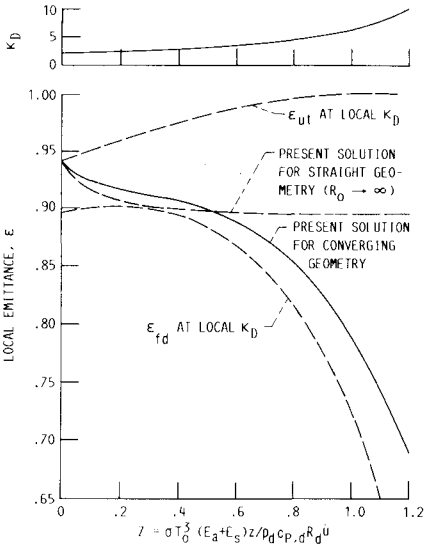

a) $R_o = 1.5$, $\kappa_{D,o} = 2$, $\Omega = 0$

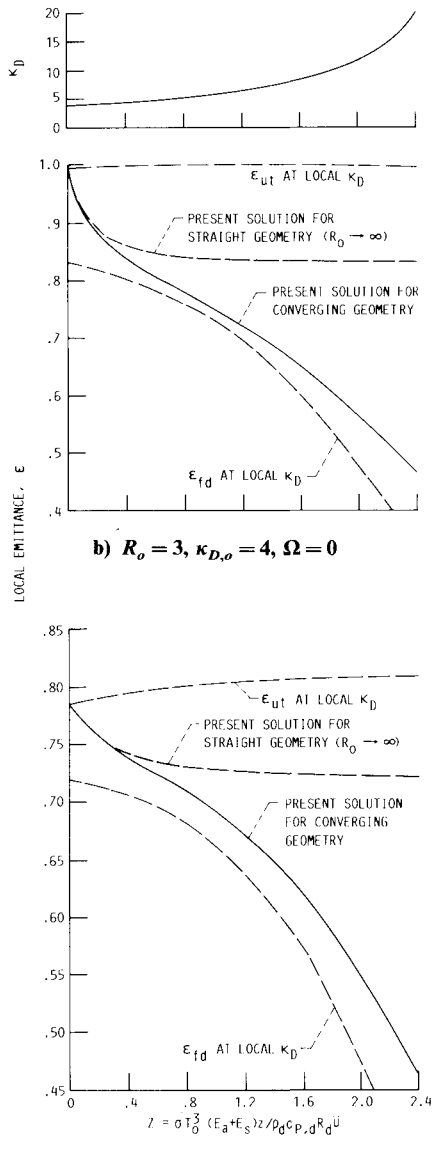

b) $R_o = 3$, $\kappa_{D,o} = 4$, $\Omega = 0$

c) $R_o = 3$, $\kappa_{D,o} = 4$, $\Omega = 0.6$

Fig. 6 Local emittance along the length of a converging droplet layer.

distribution at $\kappa_D(Z)$, which is reached during transient cooling in very low temperature surroundings. Early in the cooling process, the effect of layer convergence is small, and the solution follows the emittance curve for a straight geometry. As the outermost regions cool and the temperature distribution begins to develop, the emittance tends to follow the lowest curve, which is for the fully developed temperature solution at each Z. The results cannot reach the lowest curve because the κ_D continues to increase, and the adjustment in the temperature distribution lags behind the equilibrium shape. Although the emittance can consequently decrease considerably as Z increases, its effect is somewhat diminished in the results for local mean temperature for the following two reasons. The rate of energy loss for larger Z values decreases substantially because of the decrease in $T_m^4(Z)$; hence, the higher ε values early in the cooling process are the most important. As Z increases, the geometry converges and the external surface area is reduced. This also tends to accentuate the importance of the higher ε values at the small values of Z.

Concluding Remarks

Radiative cooling has been analyzed for a converging radiating medium with an increasing optical thickness, and the results were compared with those for a nonconverging geometry. In the converging geometry, the cooling rate was reduced by the decrease in external surface area and by the increase in optical thickness of the medium. The latter caused a reduction in layer emittance during transient cooling because of the relatively large cooling of the outermost regions. The resulting lower temperatures in the most exposed portion of the layer reduced the layer emittance, which is based on the much higher mean temperature of the layer. Results for the cooling of the layer were compared with those calculated by using local emittance values for a layer at uniform temperature with the same local values of the optical thickness. For initial optical thicknesses up to about two, this procedure gave results that were quite close to those from the present numerical solution. For larger optical thicknesses the agreement is not as good, but is somewhat improved if the scattering is large. Hence, the simplified solution is a useful approximation that can be used for some conditions of optical thickness and scattering albedo.

References

[1]Mattick, A. T. and Hertzberg, A., "Liquid Droplet Radiators for Heat Rejection in Space," *Journal of Energy*, Vol. 5, Nov.–Dec. 1981, pp. 387–393.

[2]White, K. A., III, "Liquid Droplet Radiator Development Status," AIAA Paper 87-1537, July 1987; also, NASA TM-89852.

[3]Siegel, R., "Transient Radiative Cooling of a Droplet-Filled Layer," *Journal of Heat Transfer*, Vol. 109, Feb. 1987, pp. 159–164.

[4]Siegel, R., "Separation of Variables Solution for Non-Linear Radiative Cooling," *International Journal of Heat and Mass Transfer*, Vol. 30, May 1987, pp. 959–965.

[5]Viskanta, R. and Bathla, P. S., "Unsteady Energy Transfer in a Layer of Gray Gas by Thermal Radiation," *Zeitschrift fuer Angewandte Mathematik und Mechanik*, Vol. 18, May 1967, pp. 353–367.

[6]Viskanta, R. and Anderson, E. E., "Heat Transfer in Semitransparent Solids," *Advances in Heat Transfer*, Vol. 11, edited by T. F. Irvine, Jr. and J. P. Hartnett, Academic Press, New York, 1975, pp. 317–441.

[7]Siegel, R. and Howell, J. R., *Thermal Radiation Heat Transfer*, 2nd ed., Hemisphere Publishing, Washington, DC, 1981.